



Fermi National Accelerator Laboratory

FN-369
2330.000

ORBIT TRACKING STUDIES FOR THE TEVATRON

A. D. Russell

June 1982



Operated by Universities Research Association Inc. under contract with the United States Department of Energy

Orbit Tracking Studies for the Tevatron

A.D. Russell

Fermi National Accelerator Laboratory
P.O. Box 500
Batavia, Illinois 60510

1. Introduction

In this note I will describe briefly two programs that have been written for tracking studies^{1,2} as part of the Tevatron design effort and illustrate their application with a few examples. These programs are fundamentally similar, differing primarily in details related to application. Except where stated, this note is based on the one I have written.

Central to both these programs is an attempt to foresee problems that may be caused by the non-linear multipole components in the Tevatron magnets. (The mechanical complexity of four miles of cryostat in our ring of superconducting magnets makes it unpleasant to contemplate corrections requiring substantial movements of magnets or the addition ad hoc of new correction elements.) We address these questions by including in the programs rather detailed descriptions of the multipole content of the fields of the dipole and quadrupole magnets. Normal and skew terms through 30-pole are included for the dipoles and through 12-pole for the quadrupoles. Multipole coefficients through 12-pole are assigned independently for each magnet. Above 12-pole, only the average values are used.

The program takes ~60 ms of Cyber 175 cpu time to calculate one particle through one turn. Consequently, its use has been restricted to questions encountered on time scales of at most a few hundred turns.

2. Program Description

The approach used in these programs is straight forward. Each particle is projected through the lattice elements sequentially. Non-linear terms in the guide fields are approximated as impulses added at the middle of each linear element (dipoles and quadrupoles). Correction elements are included as thin lenses.

The program has been coded to emphasize speed of execution. To this end we exploit the high degree of regularity in the Tevatron: all 774 dipoles are identical and excited to a common field; the few varieties of quadrupoles differ only in their effective lengths. The dipoles are described as sector magnets³ with all circular functions approximated to lowest order in the bend angle. The quadrupoles are described by the standard 2 x 2 matrices. Fringe fields are neglected.

The inclusion of such a large number of multipoles in each dipole and quadrupole dominates the computation time for the program. Very efficient code for evaluating these terms is based on the standard nested factorization algorithm for evaluating polynomial functions⁴. If we write the multipole expansion

$$B_y + iB_x = B_0 \sum_{n=0}^N (b_n + ia_n)(x + iy)^n$$

then the algorithm may be written

```
R = bN, S = aN, n = N
```

```
do while (n ≥ 0)
```

```
  n = n-1
```

```
  T = Rx - Sy + bn
```

```
  S = Sx + Ry + an
```

```
  R = T
```

```
end do
```

$$B_y = B_0 R$$

$$B_x = B_0 S$$

In practice, the particle motion is studied with respect to a closed orbit. With the inclusion of the non-linear multipole terms in the guide field, it is necessary to solve for the closed orbit by iteration. A solution by Newton's method⁴ is easily formulated as follows. At some point in the lattice, let the lattice define a mapping that carries the (transverse) phase space co-ordinates after n turns, $\vec{x}(n)$, into those after $n+1$ turns, $\vec{x}(n+1)$:

$$\vec{x}(n+1) = \vec{f}(\vec{x}(n))$$

$$\vec{x} = (x, x', y, y')$$

The closed orbit satisfies

$$\vec{x}(n+1) = \vec{x}(n)$$

Taylor expand $(\vec{x} - \vec{f}(\vec{x}))$ around $\vec{x}(n)$ to obtain

$$x_i(n+1) - f_i(\vec{x}(n+1)) = x_i(n) - f_i(\vec{x}(n))$$

$$+ \left(\hat{c}_{ij} - \frac{\partial f_i}{\partial x_j} \bigg|_{\vec{x}(n)} \right) (x_j(n+1) - x_j(n)) + \dots$$

Then writing the Jacobian matrix of the mapping

$$J(\vec{f}, \vec{x}) = \left(\frac{\partial f_i}{\partial x_j} \bigg|_{\vec{x}} \right),$$

setting the left hand side to zero, and retaining only the linear terms,

$$x_i(n+1) = x_i(n) - \left(1 - J(\vec{f}, \vec{x}(n)) \right)_{ij}^{-1} (x_j(n) - f_j(\vec{x}(n)))$$

defines an iteration scheme which gives the closed orbit co-ordinates.

The Jacobian matrix obeys a chain rule and can be built up from the explicitly calculable Jacobian matrices for each element in the lattice. As an immediate consequence of the closed orbit calculations, the Jacobian matrix evaluated on the closed orbit is the one turn transfer matrix for the (coupled) small amplitude betatron oscillations about the closed orbit⁵.

The implementation of Newton's method is found to converge very rapidly, usually taking a few iterations to yield a numerically stable solution for the closed orbit.

Coupling of the horizontal and vertical betatron oscillations is included naturally in this calculation. The tunes of the normal modes are given by the eigenvalues of the transfer matrix, but the correct description of the betatron functions is a more complex problem. Simply as a working hypothesis, I have assumed that the normal modes are "close" to horizontal and vertical and that the betatron functions can be approximated by the same elements of the transfer matrix as in the uncoupled case and the correct tunes, so long as the coupling is relatively small.

3. Results

To see the effects of the multipole components in the fields of the dipole magnets, four sets of multipole coefficients for the 774 dipoles were selected from normal distributions based on measured magnet data and the machines so defined, studied. No significant differences between the four cases were found. The representative results presented here are based on one set only. Some recent multipole data for 526 dipoles are given in Table 1.

The layout of the Tevatron ring is shown in Figure 1. The six long straight sections in the ring are centered at the " \emptyset " locations. The high- β insertions at the A and D sector long straight sections are needed for extraction. The electric and magnetic extraction septa are located at high- β

points just upstream of D \emptyset and A \emptyset , respectively. Except as noted, results that depend on azimuth are calculated at the middle of the C \emptyset long straight section.

Substantial non-linear multipole terms are inherent in the design of the Fermilab superconducting dipoles (Table 2). The momentum aperture of a ring of such magnets is therefore the best one can hope for. Figure 2a shows tune versus $\delta p/p$, the fractional deviation from the nominal beam momentum, for this case. The natural chromaticity has been set to zero, using the trim sextupoles. The useful momentum aperture is about $\pm 0.35\%$.

The same calculation was made using the generated multipole distributions. For this example, the correction circuits were tuned to maximize the useful momentum aperture. The tunes, Figure 3a, are found to be sensibly constant for $\delta p/p$ in the range of $\pm 0.1\%$. For comparison, the momentum spread of the beam to be injected into the Tevatron from the Fermilab Main Ring is expected to be $\pm 0.025\%$. The limits implied by the tune vs $\delta p/p$ curves are echoed by the plots of beta versus $\delta p/p$, Figures 2b and 3b.

To examine the magnetic aperture of the lattice one can track a particle started with given displacement from the closed orbit through some number of turns. The maximum amplitude for which the particle displacement remains bounded (no apertures other than the magnetic fields being imposed) defines the magnetic admittance. Figure 4 shows the case of a particle initially displaced by $250 \mu r$ in x' from the closed orbit and tracked through 128 turns. The x admittance is estimated from Figure 4a to be $4.6\pi \mu m \cdot r$. The area of yy' phase space shown in Figure 4b ($\sim 1.4 \mu m \cdot r$) is the region explored because of x - y coupling. The y admittance estimated by giving the test particle an initial displacement in the y direction is $\sim 4\pi \mu m \cdot r$. For comparison, the transverse emittances of the beam to be injected are estimated to be $0.15\pi \mu m \cdot r$ at 150 GeV.

The problem of controlling coupling of the betatron oscillations is of considerable concern to the Tevatron. Figure 5a shows the boundary in x phase space corresponding to $\epsilon_x \approx 0.2\pi \mu\text{m}\cdot\text{r}$. Figure 5b shows the area explored in y phase space ($\sim 0.002\pi \mu\text{m}\cdot\text{r}$) when the correction circuits are tuned to minimize coupling. (Note that the scales in the x and y phase space plots are different.) For Figure 6, the coupling correction was reduced by 40%. The dramatically stronger coupling is shown by the distortion of the ellipse boundary in Figure 6a and by the 27-fold increase in area explored in y-phase space ($\sim 0.054\pi \mu\text{m}\cdot\text{r}$), Figure 6b.

The preceding examples have looked at behavior near a stable operating point ($\nu_x = 19.435$, $\nu_y = 19.405$). To look near the half-integer extraction resonance, ν_x is moved into the stopband at $\nu_x = 19.5$ and the 39th harmonic quadrupole and octupole elements are tuned to drive a growing x amplitude. Figure 7a shows the separatrix that develops from an initial particle displacement of $\delta x' = 1 \mu\text{r}$. Note especially that, except for the few points at greatest x amplitude ($|x| > 1 \text{ cm}$), the y amplitude, Figure 7b, remains less than 0.5 mm. The extraction magnetic septum is located near A \emptyset , where $\beta_x = 245 \text{ m}$. The data shown in this example was recorded at C \emptyset , where $\beta_x = 73 \text{ m}$. An oscillation amplitude of 11 mm at the septum corresponds to an amplitude of 6 mm ($= 0.24''$) at C \emptyset . This limit is indicated in Figure 7a.

Harrison¹ has used very similar code in his Monte Carlo study of fast resonant extraction from the Tevatron. His model adds to the regular lattice the electrostatic and magnetic septa located at the high-beta points upstream of D \emptyset and A \emptyset respectively, and fast pulsed quadrupoles. The beam is brought near the extraction resonance by adjusting the slow elements (39th harmonic quadrupole and octupole circuits, for extraction at $\nu_x = 19.5$) and then driven into the stopband by the fast pulsed quadrupoles. The height of the 3 ms half sine wave pulse is adjusted to give a 1 ms spill.

The initial particle distributions were generated at $F\emptyset$ and assume $\epsilon_x = \epsilon_y = 0.15 \mu\text{m}\cdot\text{r}$ (95%) and $|\delta p/p| < 0.25\%$. These distributions are shown in Figures 8a and 9a. Evolution of the phase space of the beam at the upstream end of the magnetic septum is shown in Figures 8b - 8g and 9b - 9d. To construct these plots, the co-ordinates of the particles were recorded at each pass past the location of the magnetic septum for 4 or 5 turns preceding the time shown. The results of this simulation confirm that coupling and other effects of the nonlinear multipole terms can be adequately controlled during extraction.

References

1. M. Harrison, Fermilab internal report UPC-115; and, private communication
2. A.D. Russell, Fermilab internal reports UPC-124, UPC-141 and UPC-142
3. K.G. Steffen, High Energy Beam Optics, Interscience, New York, 1965
4. B. Carnahan, H.A. Luther, J.O. Wilkes, Applied Numerical Methods, John Wiley, New York, 1969
5. E.D. Courant, H.S. Snyder, Ann. Phys. 3, 1 (1958)

Multipole	n	$b_n \times 10^4$	$a_n \times 10^4$
4	1	0.10 ± 0.63	0.21 ± 0.73
6	2	1.40 ± 3.71	0.50 ± 1.36
8	3	-0.27 ± 0.87	-0.05 ± 1.78
10	4	-0.86 ± 1.65	-0.04 ± 0.54
12	5	-0.05 ± 0.37	-0.10 ± 0.71
14	6	7.34 ± 0.71	0.19 ± 0.43
16	7	0.00 ± 0.38	0.20 ± 0.48
18	8	-17.16 ± 0.80	-0.76 ± 0.99
20	9	-0.01 ± 0.36	0.61 ± 0.42
22	10	5.25 ± 0.49	0.31 ± 0.44
24	11	0.01 ± 0.28	-0.44 ± 0.33
26	12	-1.12 ± 0.31	-0.06 ± 0.31
28	13	-0.03 ± 0.24	0.11 ± 0.24
30	14	-0.12 ± 0.33	-0.04 ± 0.25

Table 1. Means and standard deviations of multipole coefficients from measurements on 526 Tevatron dipole magnets. Units are (inch)⁻ⁿ.

Multipole	n	$b_n \times 10^4$
6	2	0.04
10	4	1.04
14	6	4.44
18	8	-12.09
22	10	3.63
26	12	-0.82
30	14	0.07
34	16	0.03
38	18	-0.04

Table 2. Design multipole structure of Tevatron superconducting dipoles. Units of (inch)⁻ⁿ.

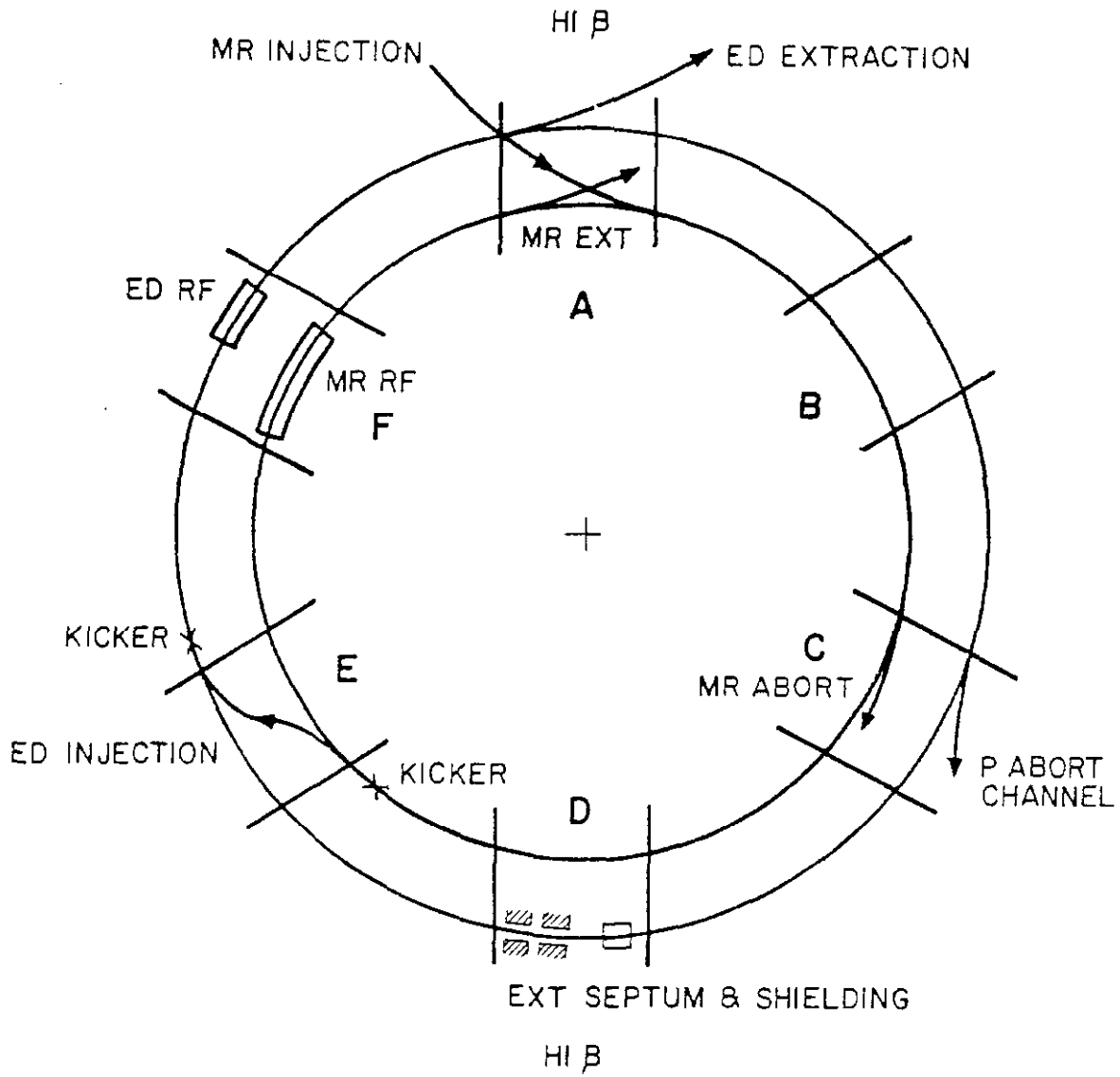


Figure 1 Layout of the Tevatron showing use of the six long straight sections.

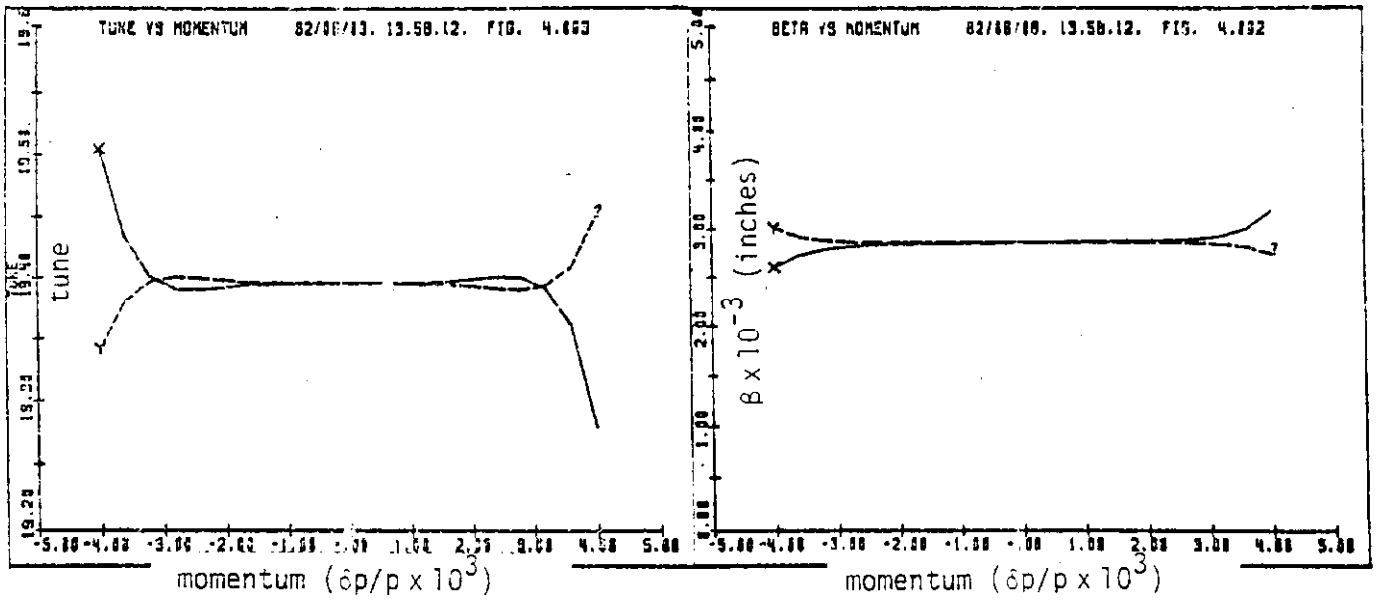


Figure 2 Tune and beta versus momentum deviation. Only the nonlinear multipoles required for the dipole design are included.

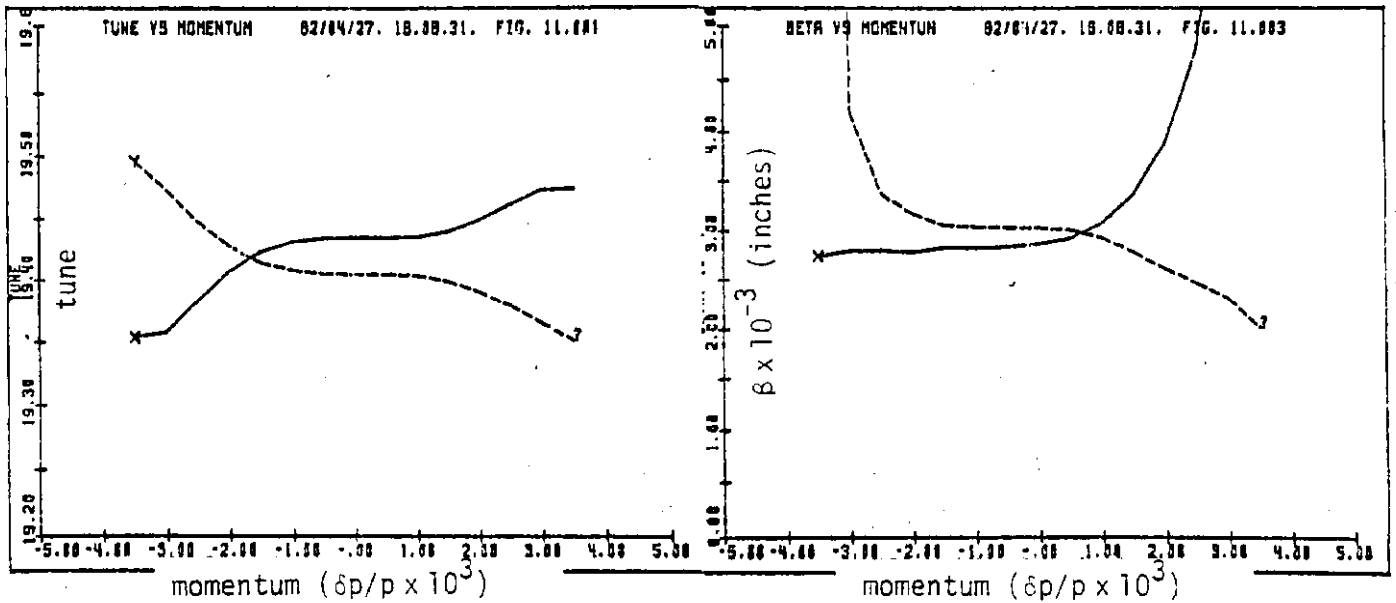


Figure 3 Tune and beta versus momentum deviation. All multipole harmonics as determined from measurements of production dipoles are included.

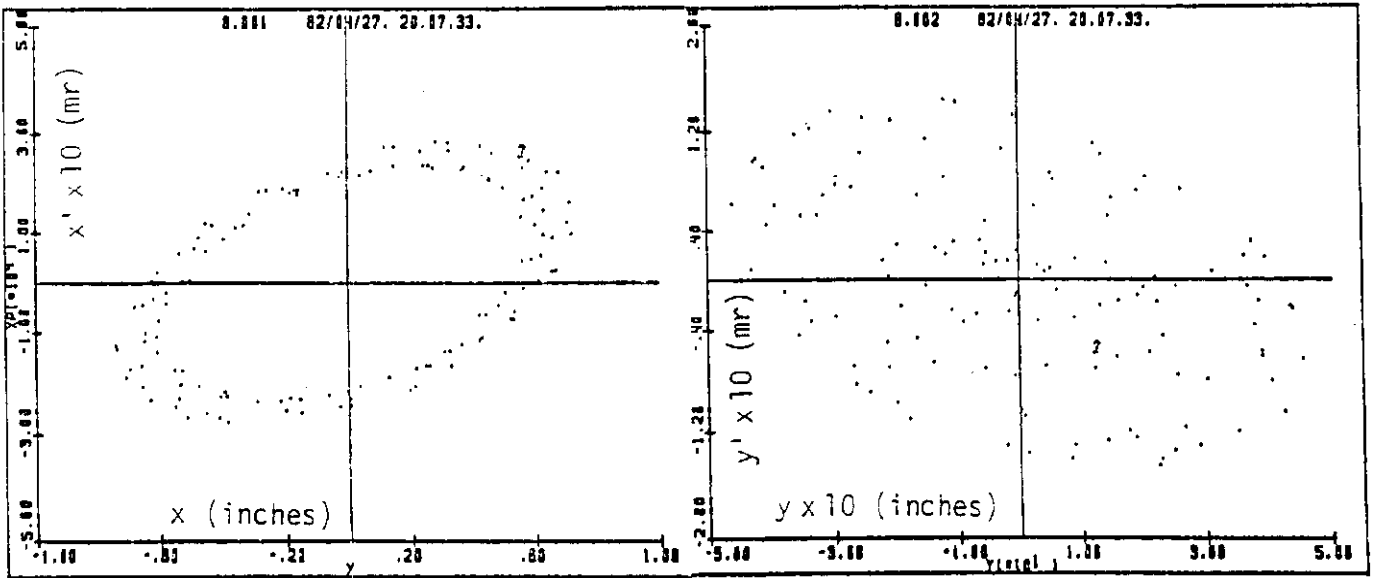


Figure 4 Phase space distributions from a particle initially displaced by $250 \mu\text{r}$ in x' from the closed orbit. Indicates the aperture limit imposed by the magnetic field structure.

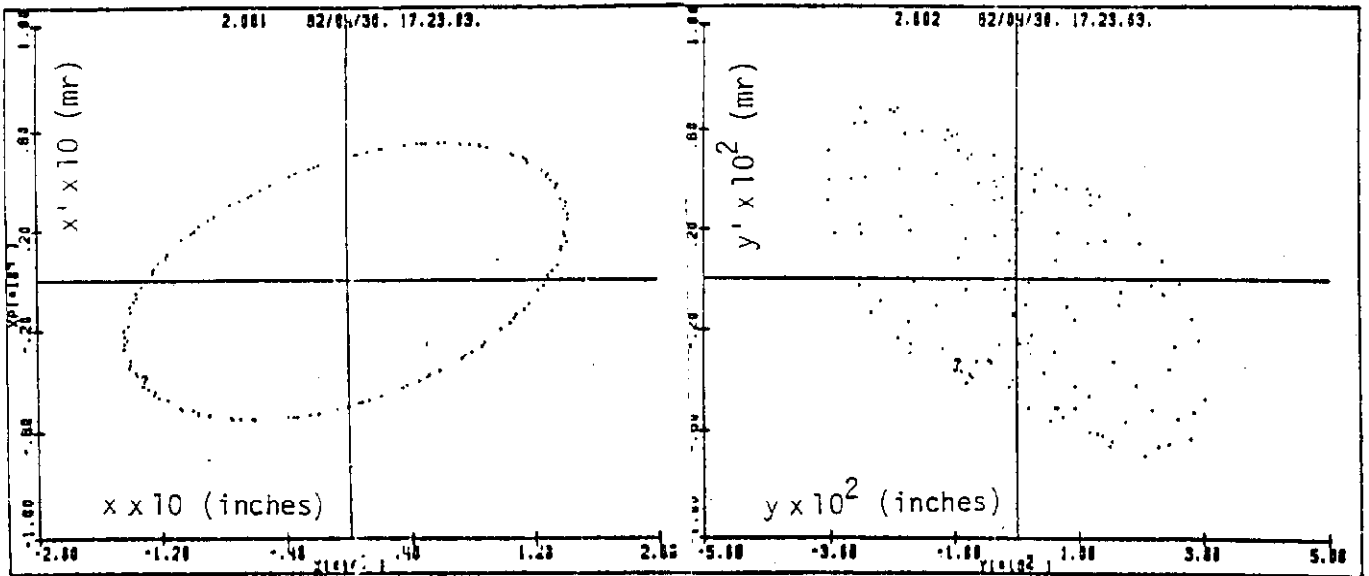


Figure 5 Phase space distribution from a particle initially displaced by $50 \mu\text{r}$ in x' from the closed orbit, corresponding to $\epsilon_x = 0.2\pi \mu\text{m}\cdot\text{r}$. The y distribution results from x - y coupling and corresponds to an effective emittance $\epsilon_y \approx 0.002\pi \mu\text{m}\cdot\text{r}$.

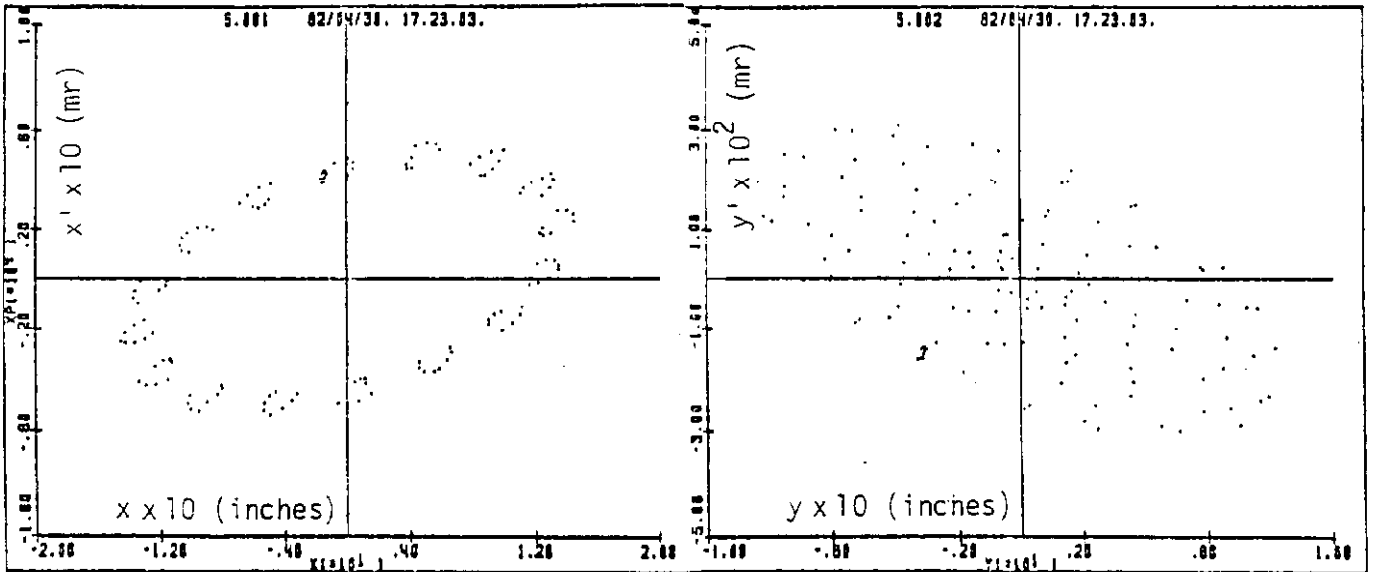


Figure 6 Same conditions as Figure 5 except that strength of skew quadrupole correction is reduced by 40%. While ϵ_x does not change, the y emittance has grown to $\epsilon_y \approx 0.054\pi \mu\text{m}\cdot\text{r}$ as a result of the coupling.

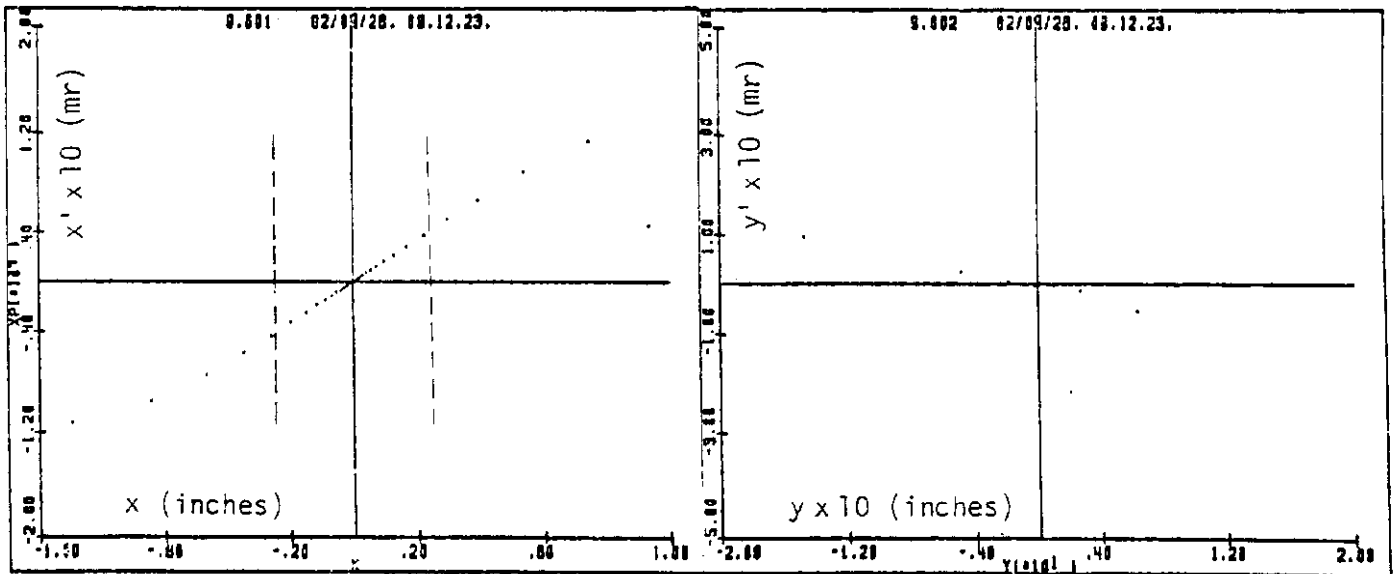


Figure 7 An example of the separatrix generated at $C\emptyset$ under conditions suitable for extraction using the half integer resonance. The dashed lines indicate the amplitude at $C\emptyset$ corresponding to the edge of the magnetic septum.

13.58.51 82/02/18.

2.50 MMS-DIV
TIME IN CYCLE 0.00
ALPHA -463
BETA 72.7

BETA*PRIME+ALPHA*(MMS)

Q0F 2.8 AMPS
Q0D -2.8 AMPS
S0F -3.5 AMPS
S0D 21.8 AMPS
H3 -2.4 AMPS
H4 15.5 AMPS
R0 -3.9 AMPS

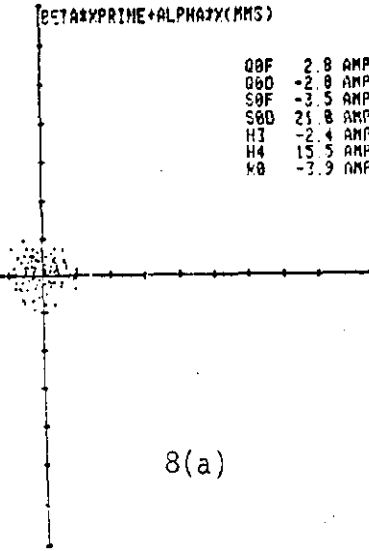
POSITION(MMS)

NORMALIZED
HORIZONTAL

CHROM 22.5
TUNE 19.465
SPO -11.5
SPK -030

Q1 -25.0 AMPS
Q3 -25.0 AMPS
H1 10.0 AMPS
H3 25.0 AMPS

FOUAD 25.0 KG-IN



8(a)

16.08.13 82/02/18.

5.00 MMS-DIV
TIME IN CYCLE 1.12
ALPHA 3.190
BETA 243.4

BETA*PRIME+ALPHA*(MMS)

Q0F 2.8 AMPS
Q0D -2.8 AMPS
S0F -3.5 AMPS
S0D 21.8 AMPS
H3 -2.4 AMPS
H4 15.5 AMPS
R0 -3.9 AMPS

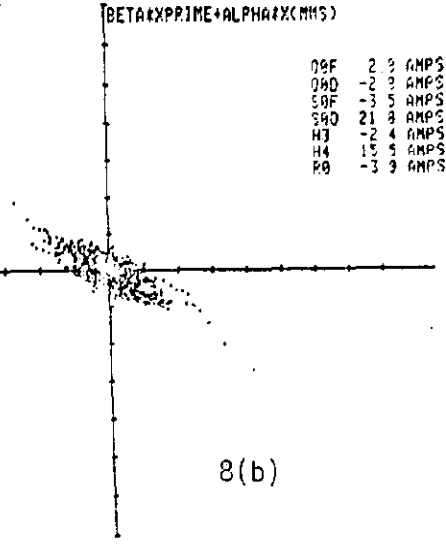
POSITION(MMS)

NORMALIZED
HORIZONTAL

CHROM 22.5
TUNE 19.465
SPO -11.5
SPK -030

Q1 -25.0 AMPS
Q3 -25.0 AMPS
H1 10.0 AMPS
H3 25.0 AMPS

FOUAD 25.0 KG-IN



8(b)

16.12.37 82/02/18.

5.00 MMS-DIV
TIME IN CYCLE 1.32
ALPHA 3.190
BETA 243.4

BETA*PRIME+ALPHA*(MMS)

Q0F 2.8 AMPS
Q0D -2.8 AMPS
S0F -3.5 AMPS
S0D 21.8 AMPS
H3 -2.4 AMPS
H4 15.5 AMPS
R0 -3.9 AMPS

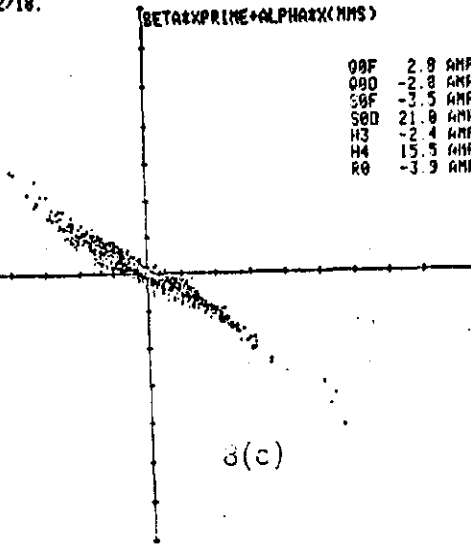
POSITION(MMS)

NORMALIZED
HORIZONTAL

CHROM 22.5
TUNE 19.465
SPO -11.5
SPK -030

Q1 -25.0 AMPS
Q3 -25.0 AMPS
H1 10.0 AMPS
H3 25.0 AMPS

FOUAD 25.0 KG-IN



8(c)

16.14.32 82/02/18.

5.00 MMS-DIV
TIME IN CYCLE 1.52
ALPHA 3.190
BETA 243.4

BETA*PRIME+ALPHA*(MMS)

Q0F 2.8 AMPS
Q0D -2.8 AMPS
S0F -3.5 AMPS
S0D 21.8 AMPS
H3 -2.4 AMPS
H4 15.5 AMPS
R0 -3.9 AMPS

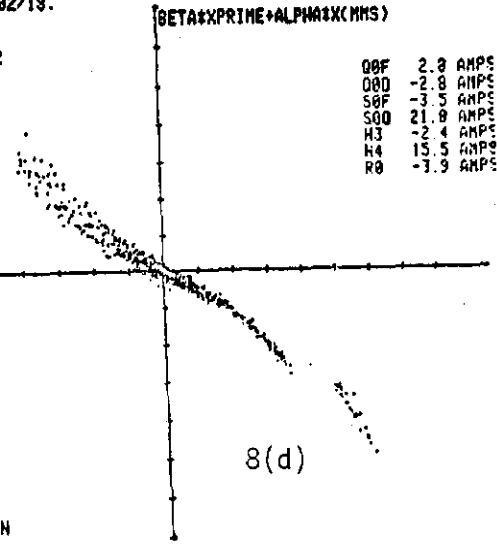
POSITION(MMS)

NORMALIZED
HORIZONTAL

CHROM 22.5
TUNE 19.465
SPO -11.5
SPK -030

Q1 -25.0 AMPS
Q3 -25.0 AMPS
H1 10.0 AMPS
H3 25.0 AMPS

FOUAD 25.0 KG-IN



8(d)

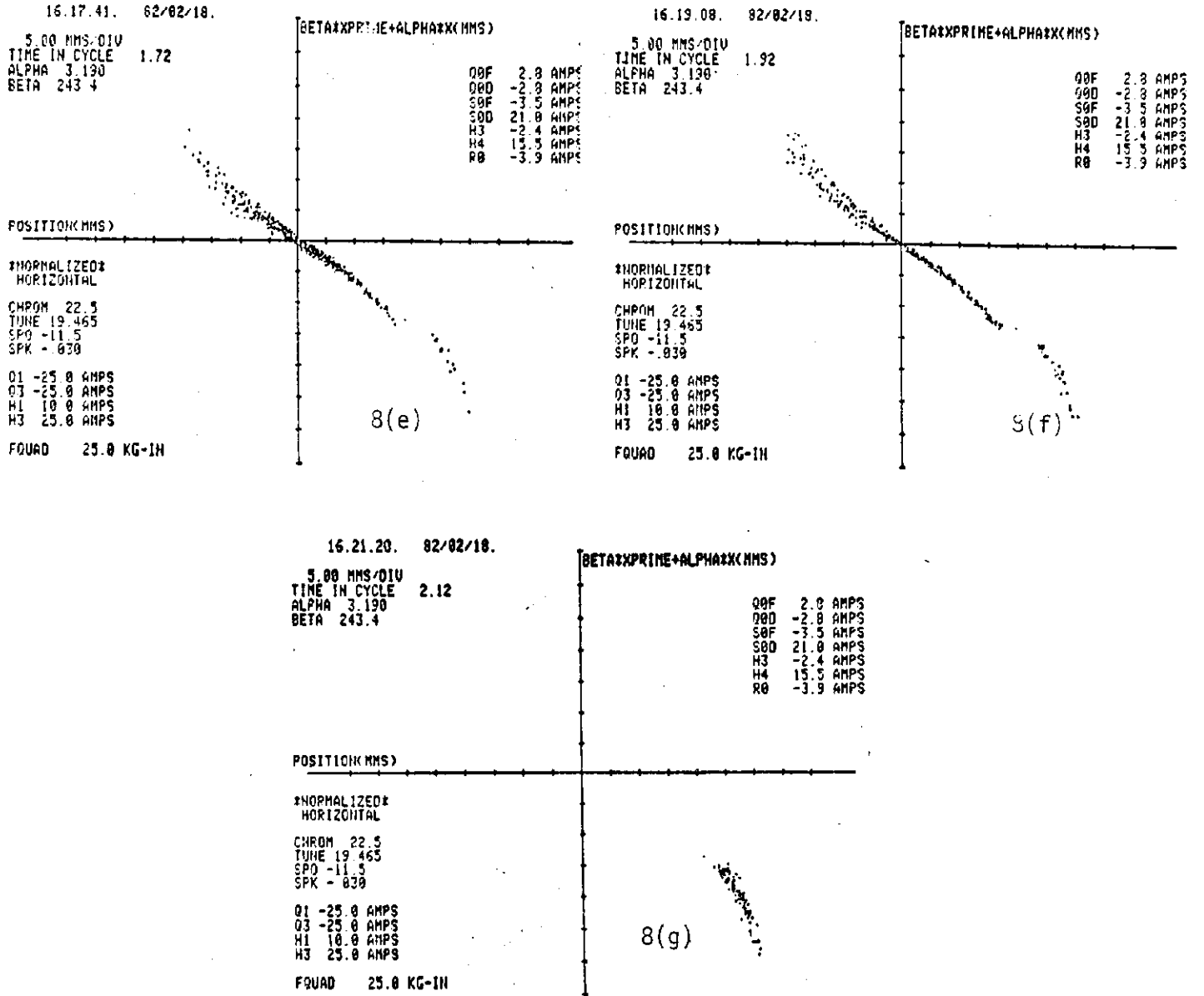


Figure 8 Phase space distributions in x from Monte Carlo simulation of fast resonant extraction. (a) Initial distribution at $F\emptyset$. (b) - (g) At upstream end of magnetic septum, as function of time.

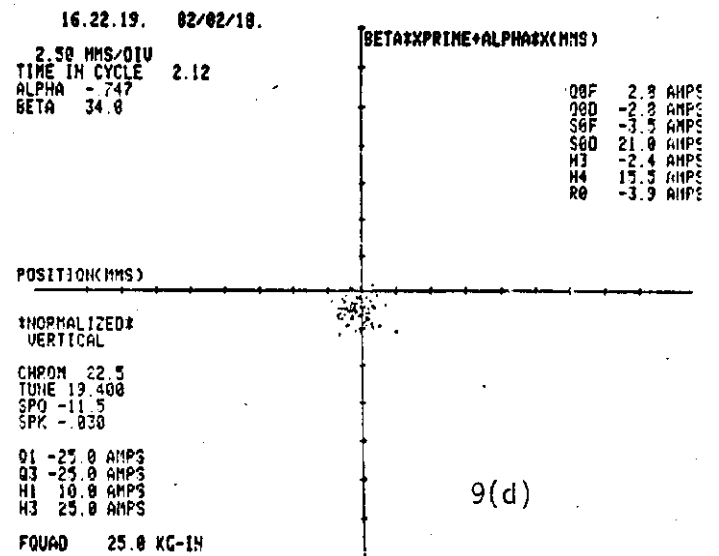
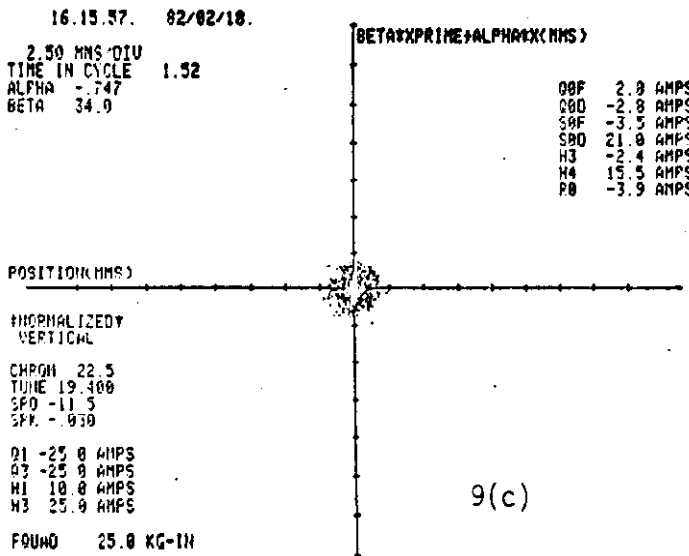
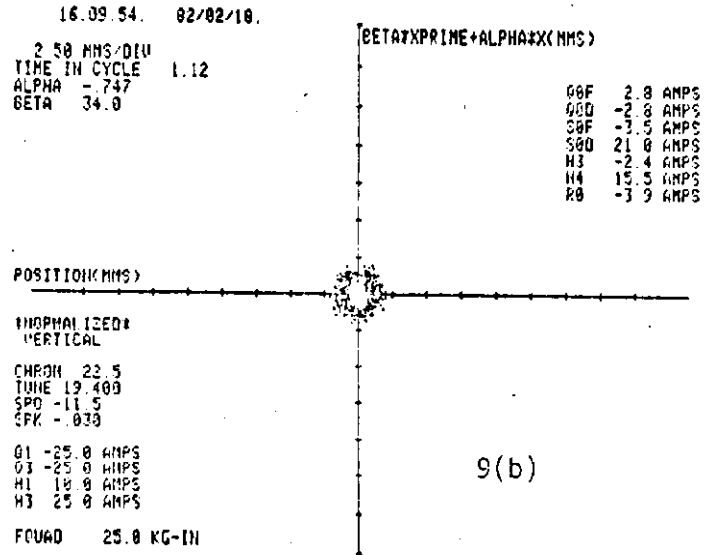
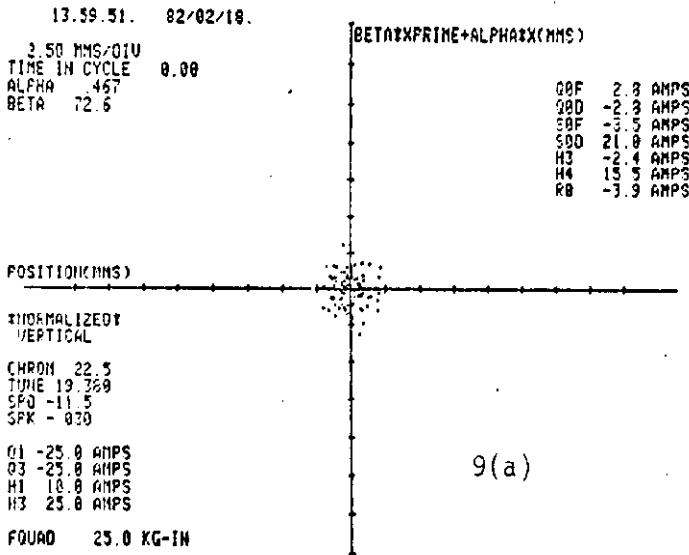


Figure 9 Phase space distributions in y from Monte Carlo simulation of fast resonant extraction. (a) Initial distribution at F0. (b) - (d) At upstream end of magnetic septum, as function of time.